PERGAMON

Journal of Structural Geology 24 (2002) 887–904

JOURNAL OF STRUCTURAL GEOLOGY

www.elsevier.com/locate/jstrugeo

Three-dimensional imaging of active structures using earthquake aftershocks: the Northridge thrust, California

S. Carena*, J. Suppe

Department of Geosciences, Princeton University, Princeton, NJ 08544, USA

Received 27 July 2000; revised 5 February 2001; accepted 18 May 2001

Abstract

Aftershocks of the 1994 Northridge earthquake (M 6.8) allow us to image the structure beneath the San Fernando Valley in northwestern Los Angeles in three dimensions. We combine aftershocks and geological data to build an image of the three-dimensional (3-D) geometry of the previously unrecognized, north-vergent Northridge blind thrust to a depth of 21 km. The most striking feature of the imaged fault is mega-corrugations oriented parallel to the mean aftershock slip vector, with most of the 1994 slip confined to west of the largest corrugation. We also image the partially overlying south-vergent San Fernando thrust, which broke to the surface in a complex rupture in 1971 (M 7.1). Both thrusts produce fault-related folding because of either fault propagation or fault bends; however, this deeper folding is masked by overlying complex deformation in the cover, which is one reason why the Northridge thrust was not identified until it ruptured in 1994. We use trishear fold modeling based on our 3-D fault geometry to evaluate possible folding due to slip on the Northridge thrust as well as its interaction with the overlapping San Fernando thrust and with shallow structures in the cover. This example illustrates the importance of earthquake data to structural geology and the value of its 3-D integration with surface and near-surface geological data.

Keywords: Earthquake; Aftershocks; Blind thrust

1. Introduction

On January 17th, 1994, an M 6.8 earthquake struck the San Fernando Valley in northwestern Los Angeles, killing 33 people and causing over $13 billion in damage (Scientists of the U.S. Geological Survey and the Southern California Earthquake Center, 1994; Fig. 1). It was determined later that the earthquake had occurred on a north-vergent blind thrust, now known as the Northridge thrust (Mori et al., 1995; Huftile and Yeats, 1996), which extends from 6 km down to a depth of 21 km beneath the San Fernando Valley. Although it is possible in some cases to identify blind thrusts based on their previous seismic activity or their associated folds (e.g. Suppe, 1983; Shaw and Shearer, 1999), this blind thrust went entirely unnoticed before 1994. Because systematic seismic monitoring began about 30 years ago, very few earthquakes were recorded in this area, none of which were large enough to warrant close examination. Careful analysis of pre-1994 seismicity later, however, revealed that at least seven earthquakes had indeed occurred on the Northridge thrust in the period 1981–1993, and these could have been used to image the approximate thrust geometry and size (Seeber and Armbruster, 1995a; Carena and Suppe 1999a).

Several attempts have been made to link overlying folds with the Northridge thrust (Davis and Namson, 1994; Yeats and Huftile, 1995; Huftile and Yeats, 1996; Tsutsumi and Yeats, 1999). Because of the complex multi-level nature of the overlying deformation, this connection is not easy to make without explicit knowledge of the deep fault geometry. Constraints on the approximate location and dip of the underlying fault were provided by cross-sections that integrated well, seismic, and surface geologic data in the shallow subsurface, and at depth by the projection of a swath of aftershocks onto the line of section (Davis and Namson, 1994; Yeats and Huftile, 1995; Huftile and Yeats, 1996; Tsutsumi and Yeats, 1999). However, we observed that when wide swaths of aftershocks are projected onto cross-sections, three-dimensionality is lost and significant distortion in the geometry can be introduced, eliminating the potential advantages of using aftershocks for characterization of three-dimensional (3-D) fault geometry. In fact, proper projection of earthquakes may be impossible without first solving for the 3-D geometry. Moreover, aftershock density is typically quite heterogeneous on faults;

* Corresponding author. Tel.: +1-609-258-1515; fax: +1-609-258-1274.
E-mail address: scarena@princeton.edu (S. Carena).

0191-8141/02/$ - see front matter
PII: S0191-8141(01)00110-9

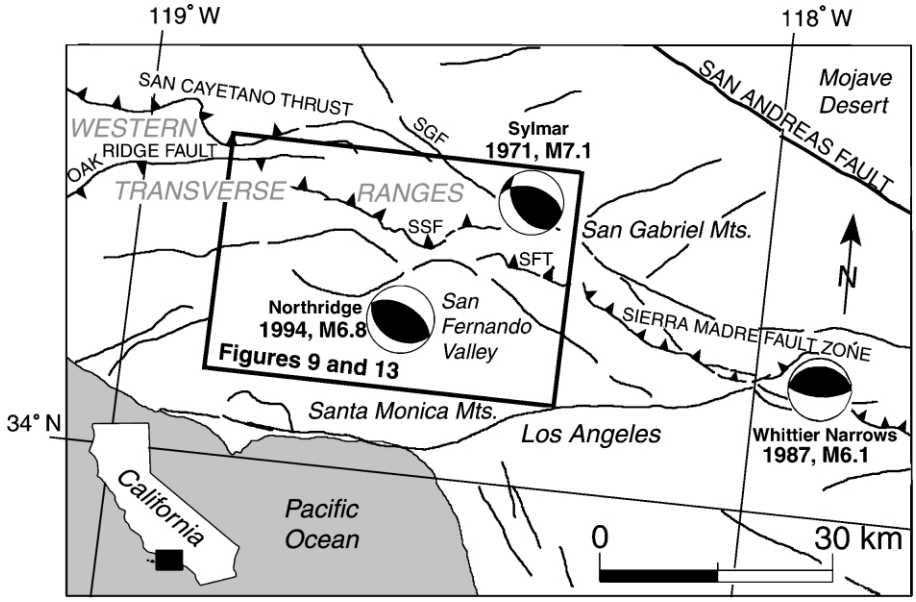

Fig. 1. Location map of the San Fernando Valley area. Note the change in fault strike from the Sierra Madre fault zone to the San Cayetano thrust. SSF = Santa Susana fault, SFT = San Fernando thrust, SGF = San Gabriel Fault.

events tend to be concentrated in specific areas such as edges of slipped patches, bends and jogs, or at fault intersections, whereas aftershocks can be sparse elsewhere (e.g. along some detachments). Thus, any interpretation of fault geometry in cross-section or map view based on projected aftershock density is inherently ambiguous.

Our approach instead is to first image the fault in 3-D directly from the locations of the aftershocks at depth. Only when necessary for purposes of two-dimensional (2-D) representation do we slice through the 3-D fault surface to produce cross-sections, onto which nearby earthquakes can be projected along the local strike of the fault. At shallow depth, where there are few earthquakes, there are other data available (e.g. stratigraphy from wells, bed dips, and seismic-reflection profiles), which we can integrate into our model. Having a 3-D fault geometry, independent from any a priori structural interpretation, helps us to discriminate in an area of complex structure between various potential interpretations based largely on data at shallow depth and 2-D swath projections of the seismicity.

2. Geologic setting

The stratigraphy is typical of the faulted south flank of the eastern Ventura rift basin, with a cover of Cenozoic and some Cretaceous sediments overlying Mesozoic and older crystalline basement (see Yeats et al., 1994; Huftile and Yeats, 1996; Tsutsumi and Yeats, 1999). The present stratigraphic thickness is quite variable in the N–S direction given the basin-flank location, but generally does not exceed 3–4 km in the San Fernando Valley based on well and seismic data (Huftile and Yeats, 1996; Tsutsumi and Yeats, 1999). Because the Northridge thrust is located between 6 and 20 km depth, most of its surface lies within the crystalline basement, as do most of the aftershocks (Unruh et al., 1997). Thus the deeper structure is dominantly basement involved; however, the structure in the cover shows significant evidence for bedding-parallel thrusts, as discussed below. How these deep and shallow deformation systems interact is a challenging question about which there is no consensus (cf. Davis and Namson, 1994; Yeats and Huftile, 1995; Huftile and Yeats, 1996; Tsutsumi and Yeats, 1999).

A major south-vergent thrust system with occasional north-vergent faults extends throughout the Transverse Ranges of California from the Sierra Madre fault zone on the northeastern flank of the Los Angeles basin to the San Cayetano thrust on the north flank of the Ventura Basin (Fig. 1). This entire thrust system shows a change in strike from NE in the south to ENE in the north. Several of these very active structures exist in and around the San Fernando Valley. The south-vergent San Fernando thrust, which ruptured the surface and caused the 1971 (M 7.1) Sylmar earthquake (Whitcomb et al., 1973; Mori et al., 1995), marks the northeastern edge of the San Fernando Valley. Its ideal continuation to the NW is the Santa Susana fault, a complex south-vergent thrust that appears segmented by at least two lateral ramps (Chatsworth Ramp and Gillibrand Canyon Ramp; Yeats et al., 1994). In 1995 Yeats and Huftile observed that the footwall of the Santa Susana fault has been uplifted since the late Pleistocene, indicating slip on an underlying south-dipping thrust. Had it been noticed earlier, this piece of evidence could have suggested the existence of a blind thrust prior to the 1994 earthquake.

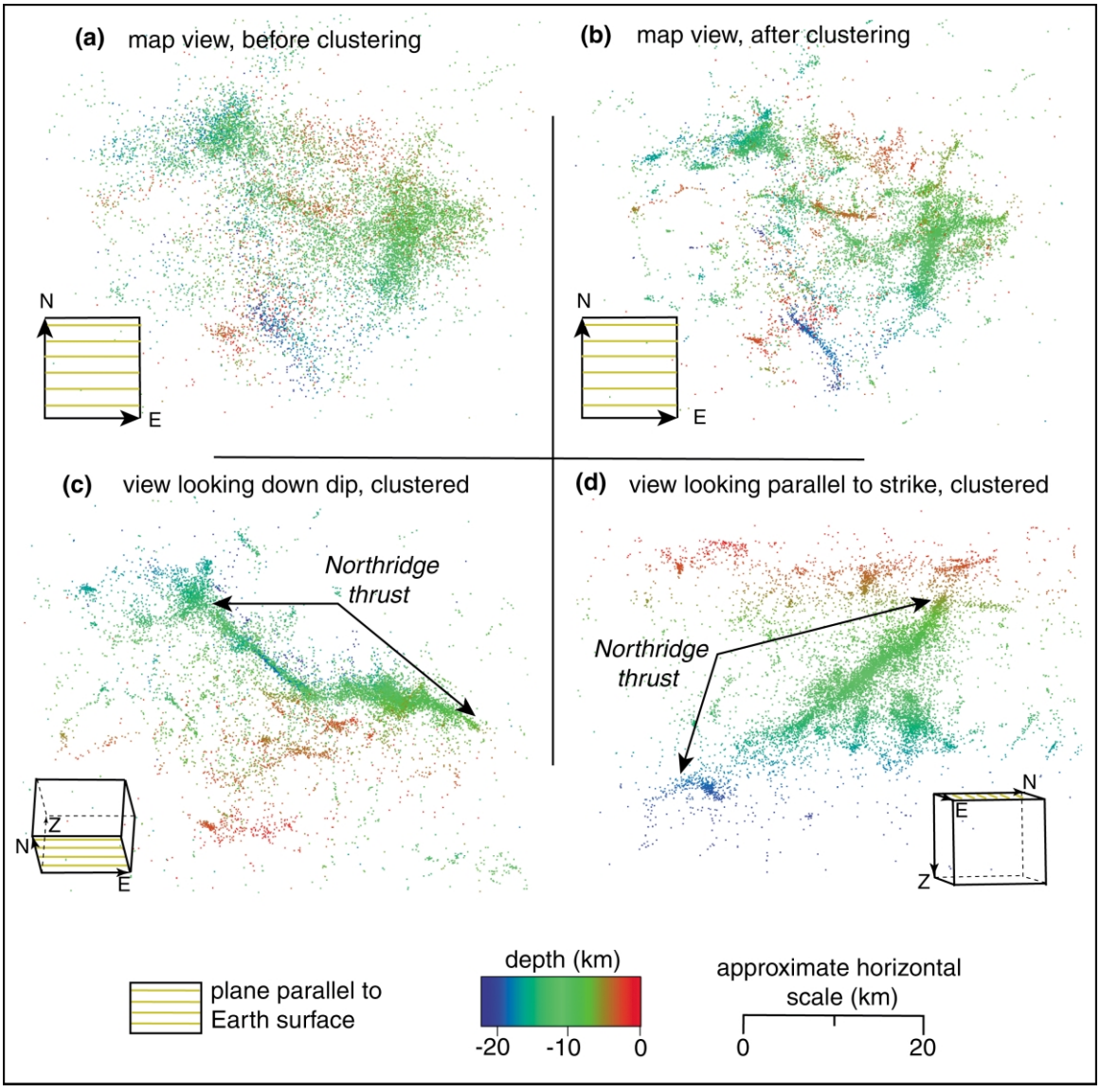

Fig. 2. Aftershock hypocenters of the 1994 Northridge earthquake, (a) unclustered and (b–d) clustered. Most of the well-defined clusters in (b) are already recognizable in (a), but their scattering is much smaller in (b). In (c) the changes in strike of the Northridge thrust are evident.

Here we examine in detail both the Northridge thrust and the San Fernando thrust, emphasizing the Northridge 3-D geometry.

3. Imaging the 3-D geometry of the Northridge thrust

Large earthquakes can produce thousands of aftershocks, many of which lie approximately on the principal fault that generated the main-shock itself (Scholz, 1990). Additionally, other aftershocks are triggered on nearby faults as a result of stress transfer. Aftershocks, because of their large numbers, are therefore an important tool for imaging the 3-D shape of a fault at depth, where little other information is available. Sequences of small events without a big shock (earthquake swarms) or, under some conditions, background seismicity also can be useful for fault imaging (Rubin et al., 1999a,b). Earthquake swarms and aftershock sequences have been integrated into 3-D structural modeling sporadically in the past (e.g. Shaw et al., 1994), but only after the Northridge earthquake were they used more extensively. For example, Seeber and Armbruster (1995a,b) have shown that blind faults in the San Gorgonio Pass and Northridge areas can be identified by viewing large sets of focal mechanisms in 3-D, and Shaw and Shearer (1999) have combined relocated aftershock data with reflection profiling to identify the source of the 1987 Whittier Narrows earthquake. To date, this kind of data has had limited use in structural geology. One reason is that the necessary 3-D software for both visualizing geologic data and earthquake locations and for building fault surface models from complex data has only recently become

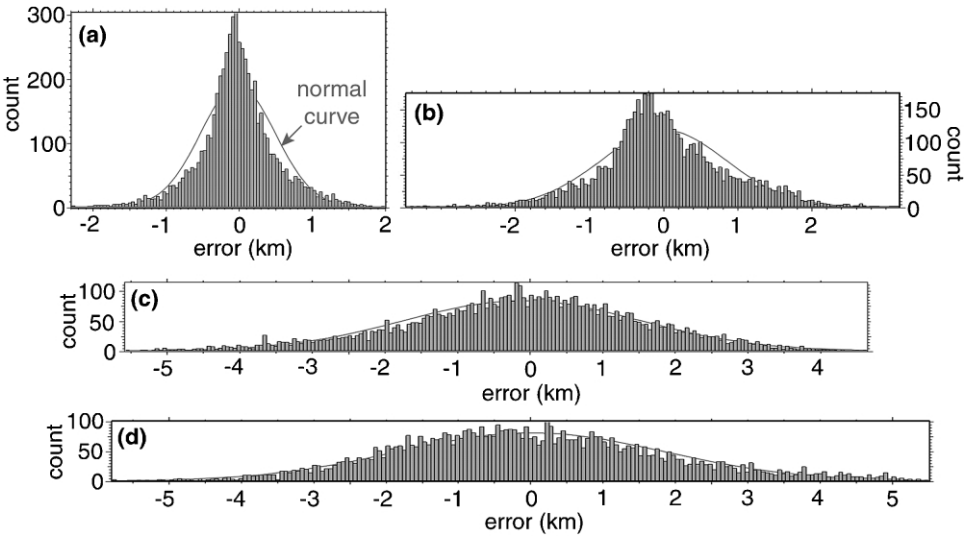

Fig. 3. Fitting statistics for the Northridge thrust. Count = number of aftershocks; error = distance of aftershock from modeled surface (negative = event is on the footwall side; positive = event is on the hanging wall side). We fit the surface modeled in Fig. 4 to the clustered hypocenter set (a), and compare it with a least-squares plane fit to the same clustered set (b). The fit in (a) is much better than in (b). If we fit the surface from Fig. 4 to the unclustered set (c), and compare it with a least-squares plane fit to the same unclustered set (d), the fit of the 3-D surface is still better than that of a plane, showing the importance of real 3-D fitting with a surface in this case. In particular, both (b) and (d) show a slight bimodal distribution, which is due to the presence of 'corrugations' in the fault surface that are ignored by a least-squares plane fitting.

available. Another factor is the quality and availability of abundant low magnitude earthquake data, which is relatively good only in some areas, like California, and even there the quality has improved enough to make the data really useful for structural geology purposes only in the last decade or so.

3.1. Method

In recent years, our group at Princeton University has experimented extensively with using aftershocks from large earthquakes to model faults by fitting surfaces in 3-D to earthquake clouds (Shaw et al., 1994; Brankmann, 1995; Van Dusen, 1997; Carena, 1999; Carena and Suppe, 1999a,b; Carena et al., 2000) within the powerful *Gocad* 3-D earth-modeling software environment (Mallet, 1992, 1997; Gocad Consortium, 2000). The procedures that we have developed and that we illustrate here with the Northridge thrust can, in principle, be applied to any high-quality data set, even though the modeling techniques generally need to be adjusted to the specific structural style and the nature of the data constraints.

We used the aftershock hypocenter locations of the 1994 Northridge earthquake to image the Northridge thrust in detail. The original data set consists of approximately 12,000 events from the SCEC database, of which about half fall on the Northridge thrust itself. The spatial pattern of these events forms scattered 'clouds' with a 2σ scatter about a fault surface on the order of a kilometer. Because of this scatter, combined with multiple faults and 3-D geometry, it can be difficult to select earthquakes from the different faults in the raw 3-D data (see Fig. 2a). The procedure described below aims at eliminating ambiguities and bringing the fault geometry into better focus.

The Northridge aftershock hypocenter locations were clustered using an algorithm by Jones and Stewart (1997) (see Appendix A for details), which makes the process of selecting subsets of earthquakes in 3-D easier and illuminates details of the fault surface otherwise masked by scattering (Fig. 2b). We next imported the clustered locations into *Gocad*, which allowed us to: (1) view the earthquakes in 3-D, (2) select subsets of hypocenters associated with different faults, (3) fit 3-D surfaces to subsets of events, and (4) obtain fitting statistics (Fig. 3). This process gave a close to Gaussian 2σ fit for the Northridge fault model of about ± 1000 m (Fig. 3a).

To begin imaging the fault, we identify clusters of earthquakes that collectively define an individual structure. We assume that disconnected quasi-planar clusters of earthquakes with different orientations represent separate structures. In the case of the Northridge aftershocks, most earthquakes belong to some specific cluster. Only a few hundred earthquakes do not belong to any cluster and look randomly scattered. All the recognizable clusters depict well-defined surfaces, instead of being composed of earthquakes uniformly scattered throughout a volume (Fig. 2). We have developed techniques to select earthquakes in each cluster and save them to separate files using tools available in *Gocad* (Gocad Consortium, 2000). We then limit our final selection for the Northridge thrust cluster to events located within ± 1.5 km from the quasi-planar region of maximum earthquake density (Fig. 2c) in the cluster itself. Since 95% of the clustered events fall within 1 km of our final fault

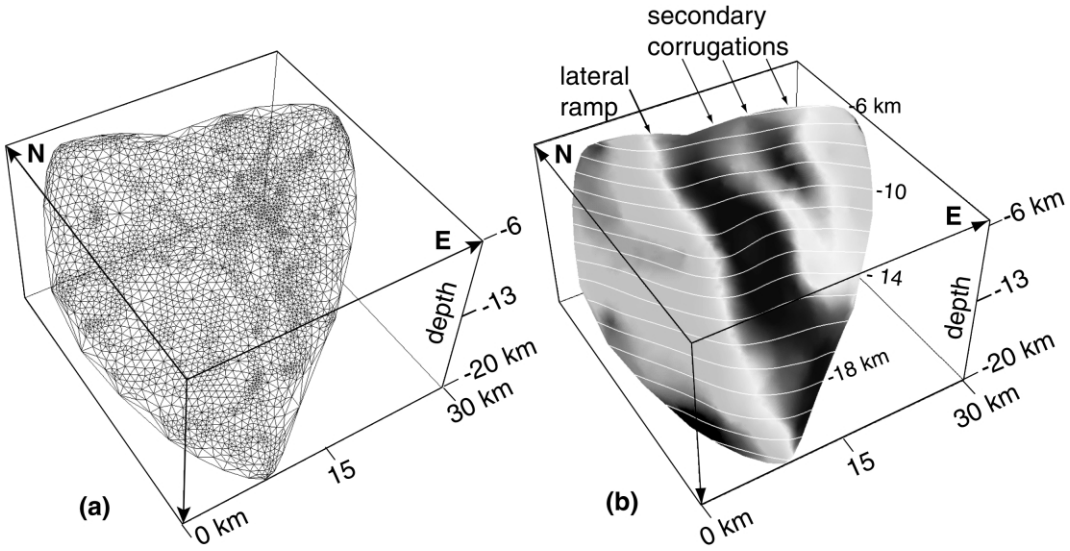

Fig. 4. Northridge thrust surface modeled from the aftershock hypocenters, after smoothing with the *Gocad* DSI algorithm. (a) Triangulated surface. (b) Depth-contoured surface (depth below sea level, contour interval 1 km), with shading to highlight fault topography. Note how the trends of the lateral ramp and of the secondary corrugations are very close.

surface (Fig. 3a), using a ± 1.5 km range means that all the events belonging to the Northridge thrust will be included. We had to use a selection range of more than 1 km (i.e. larger than 2σ) because of practical difficulties in selecting events in 3-D. Thus the final selection includes about 300 events that likely do not belong to the Northridge thrust, but as we will see, their influence on the final result is negligible.

In the general case, all the available surface breaks, focal mechanisms, well data, seismic-reflection profiles, and geological maps/cross-sections should also be imported at this stage. Surface breaks, wells, and seismic-reflection

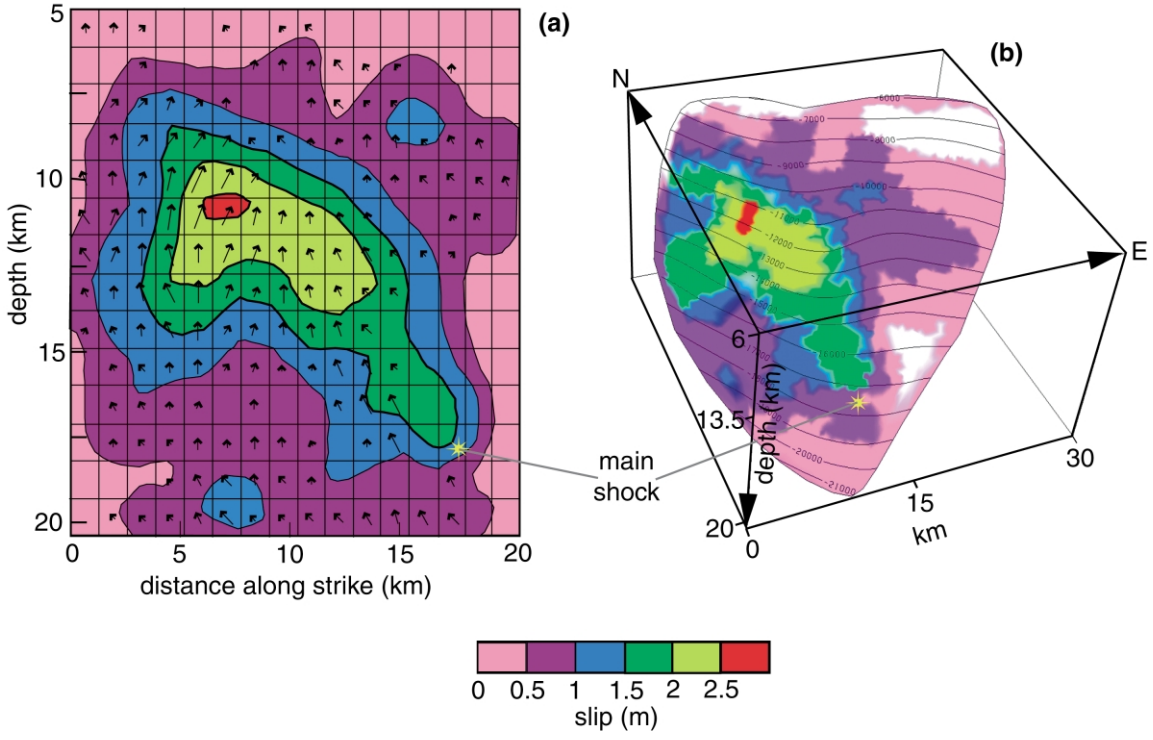

Fig. 5. (a) 2-D slip model (contours = slip magnitude, contour interval 0.5 m; arrows = slip direction at different points on the fault), modified from Wald et al. (1996), and (b) the same slip model projected onto our Northridge thrust 3-D surface. Most of the slip occurred west of the lateral ramp. Here we kept the main-shock location (star) in the pre-clustering position, because this is the location used by Wald et al. (1996) in their model.

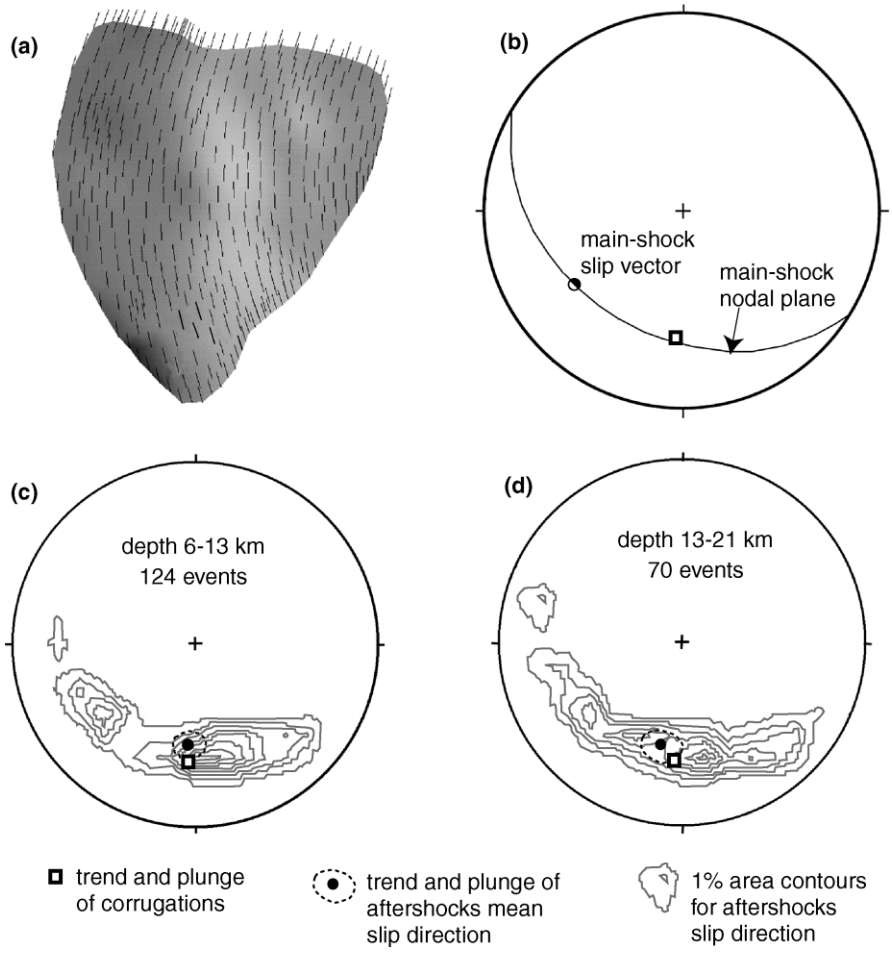

Fig. 6. Comparison among (a) the theoretical slip directions computed by Mallet et al. (1999) on the basis of fault curvature alone, (b) the trend and plunge of the corrugations, and (c, d) the trend and plunge of the aftershocks mean slip direction at two different depth ranges, with 95% confidence ellipse. The focal mechanisms used to compute the equal-area stereoplots (b–d) are from N. Seeber (SCEC database).

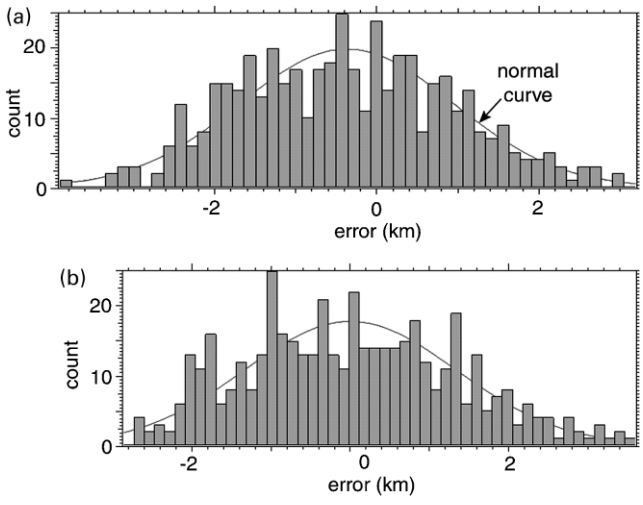

Fig. 7. Fitting statistics for the San Fernando thrust. Count = number of aftershocks; error = distance of aftershock from modeled surface (negative = event is on the footwall side; positive = event is on the hanging wall side). (a) 3-D surface fit; (b) least-squares plane fit.

profiles can be used to constrain the position of the top of a fault and may disclose a change in fault dip that could have gone undetected, because there are often only a few events at very shallow depths (0–3 km in the San Fernando Valley). These data also can provide information regarding the presence of fault splays or other shallow faults near the Earth's surface. Focal mechanisms can be used to further constrain the fault geometry; they are particularly useful when the density of hypocenters is low, and are imported in *Gocad* as nodal planes and slip vectors. The 1994 Northridge earthquake did not produce surface breaks, but we included surface breaks from the 1971 Sylmar earthquake in our model of the San Fernando thrust.

The next step is to generate fault surfaces from the identified clusters and the additional data. A cloud of earthquakes can theoretically be fit with a plane using a least-squares inversion. But such a simple linear fault model is not relevant for the purpose of building structurally realistic surfaces. In many cases real faults have a rather complex geometry that we seek to understand and in fact may be highly 3-D (e.g. Shaw et al., 1994). A least-squares fit gives the average strike and dip of the fault, but it will

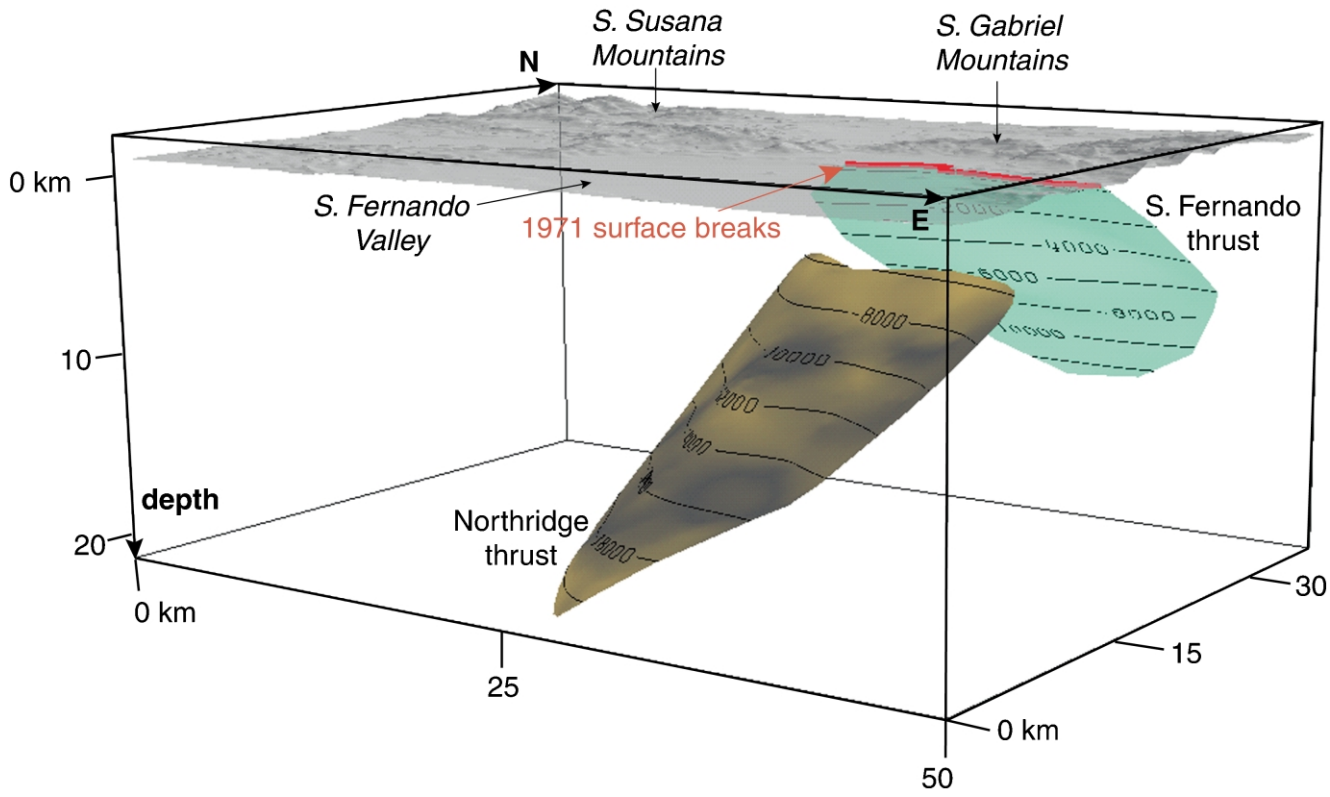

Fig. 8. Perspective view, looking from the SE, of the modeled Northridge and San Fernando thrusts. The Northridge thrust stops at a depth of about 6 km, and its upper tip east of the lateral ramp (Fig. 4) terminates almost against the San Fernando thrust, as was suggested by Mori et al. (1995). The San Fernando thrust lower tip is at a depth of 13 km, whereas the Northridge thrust lower tip is at 21 km.

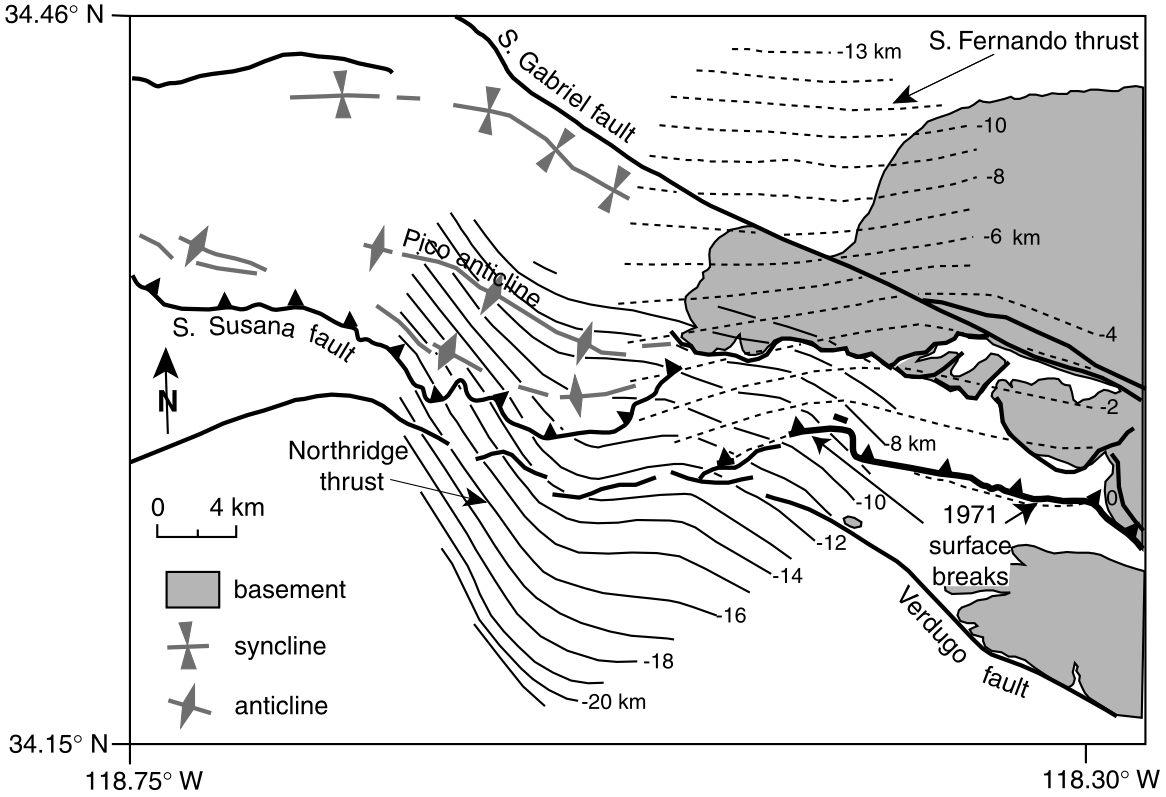

Fig. 9. Schematic geological map showing the position of the main faults and folds, as well as the depth contours (contour interval = 1 km) of the Northridge (solid) and San Fernando (dashed) thrusts.

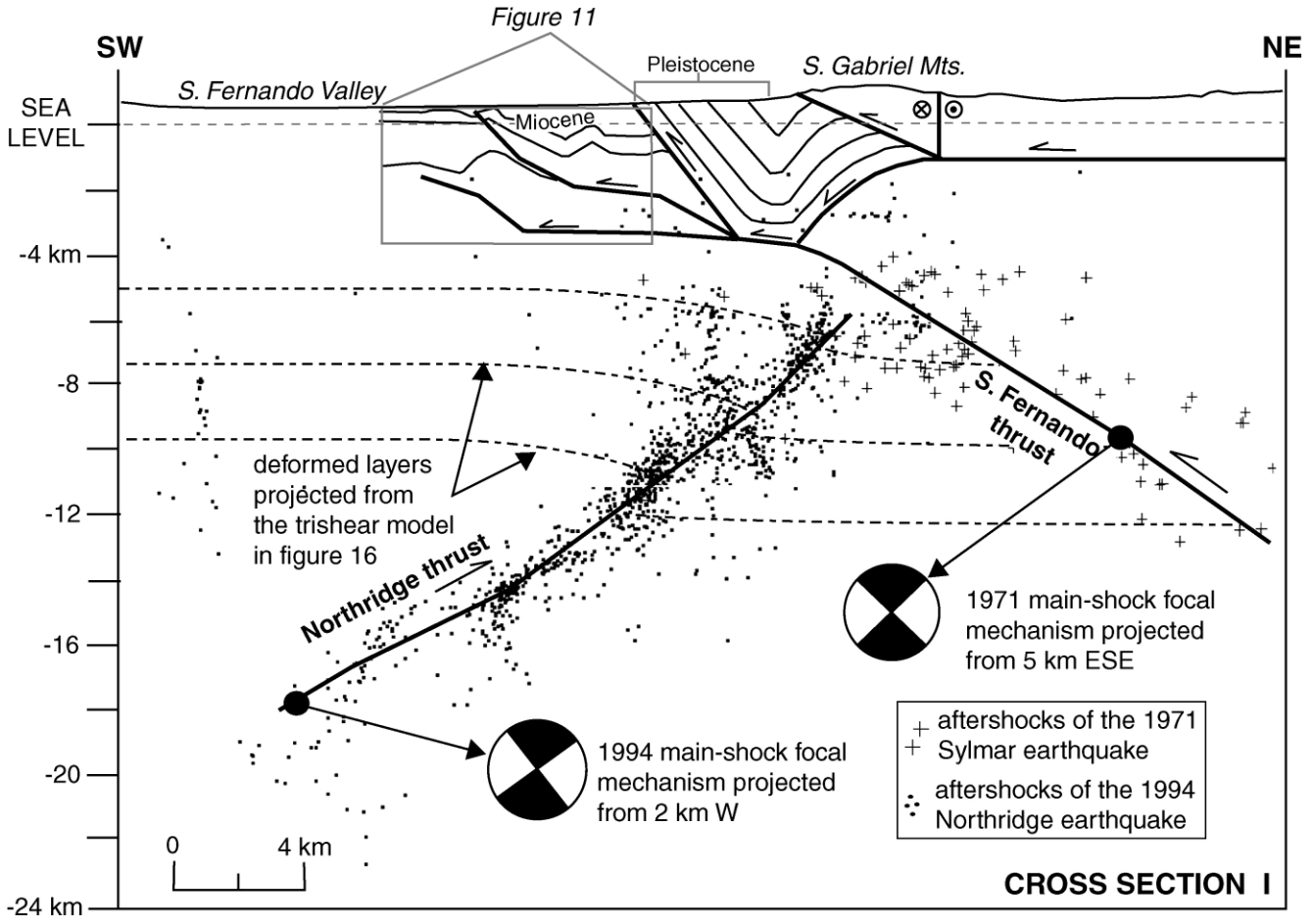

Fig. 10. Cross-section through the San Fernando Valley with projected aftershocks of the 1994 Northridge earthquake and of the 1971 Sylmar earthquake. The Northridge aftershocks are projected from a distance of 1 km or less on each side of the cross-section (main shock projected from 2 km W), whereas those of the Sylmar earthquake are projected from 1.5 km or less (main shock projected from 5 km ESE). The sources that we used for the near-surface geology and structure are Dibblee (1991) and a seismic line (Fig. 11). The large N–S changes in Upper Tertiary stratigraphic thicknesses in this region (Dibblee, 1991, 1992a), prevent detailed stratigraphic correlation across fault blocks (this figure and Fig. 12). This fact suggests that the shallow faults, and possibly the deeper San Fernando thrust itself, are reactivating old normal faults of the southern margin of the Ventura basin (Yeats et al., 1994; Huftile and Yeats, 1996; Tsutsumi and Yeats, 1999). Location of cross-section is in Fig. 13.

miss any step, bend, splay, or changes in dip (Fig. 3b and d). Not only are steps and bends often the starting point of major earthquakes and the areas where seismicity tends to concentrate, but any change in the fault orientation is a potential source of either folds or other faults (e.g. Suppe, 1983; Shaw et al., 1994; Shaw and Shearer, 1999).

To capture the true 3-D fault geometry, we use irregular triangulated surfaces (Tsurfs; Gocad Consortium, 2000) as the basis of fitting the hypocentral locations. Initially a surface is generated by connecting together all nearest neighbor earthquakes. This results in a 'jagged', highly irregular surface, which is then smoothed (Fig. 4a) with the *Gocad* DSI (discrete smooth interpolation) algorithm (see Mallet (1997) for details). Less weight is assigned during smoothing to isolated points (Mallet, 1997). Thus, the presence of a few hundred of possibly extraneous earthquakes (equal or less than 5% of the data) scattered at the outer margin of the earthquake cluster does not have an appreciable effect on the final geometry of our Northridge thrust surface model. During smoothing, 'control nodes' can be set to keep the position of specific nodes on the triangulated surface fixed. Surface breaks are a good example of data points that can be used as control nodes, when available. Our purpose is to obtain a smooth surface that preserves all the major geometric features already existing in the original earthquake cloud, while smoothing out minor 'bumps', which are likely artifacts due to either original location errors not filtered out by relocation procedures, or accidental inclusion of events not belonging to the fault. For this reason, we do not preserve any feature of the surface whose size is smaller than the mean location error in the unclustered hypocenter locations (± 700 m, which is the average of both vertical and horizontal uncertainty in event location, for Northridge).

3.2. Results: a corrugated fault surface

Our final model of the Northridge thrust is a 3-D fault

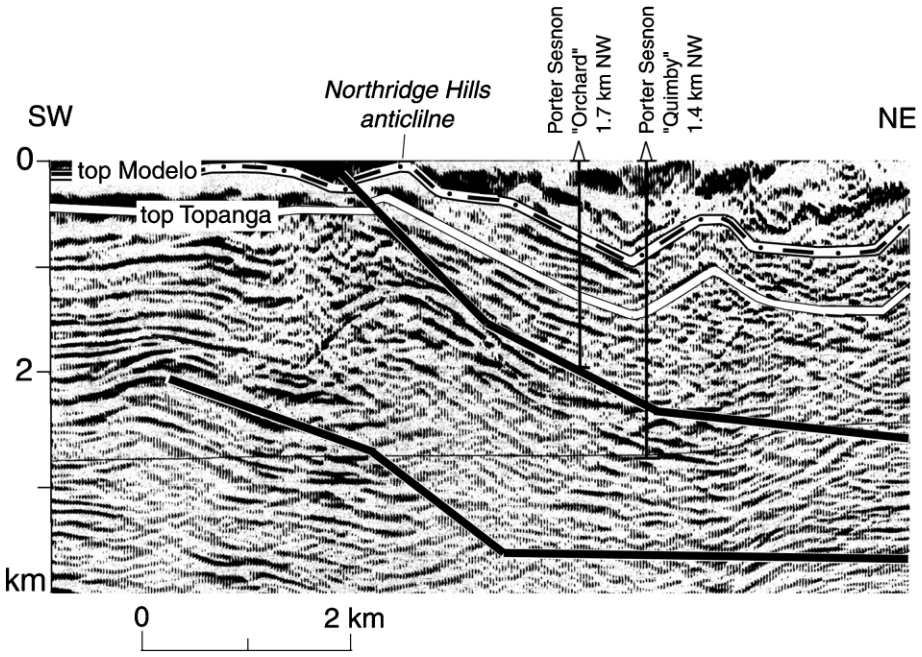

Fig. 11. Depth-migrated seismic-reflection profile oriented NE–SW in the San Fernando Valley. Two small blind thrusts can be recognized, and the anticline associated with the upper thrust corresponds to the Northridge Hills anticline of Dibblee (1991, 1992a).

surface (Figs. 4–6) with a marked lateral ramp in the middle, a minimum surface area of 450 km^2, and an upper fault tip at approximately 6–7 km depth. The strike of the surface varies from 110° east of the lateral ramp (which strikes E–W) to 130° west of it, and the average dip changes from 35° to 43°, respectively. The lateral ramp is wider at the upper fault tip, and narrows with depth; below 15 km it is reduced to a simple change in fault strike (Fig. 4b). The lateral ramp coincides with the location of a major ESE trending lineament at shallow depths (the "Chatsworth trend" of Whitcomb et al., 1973) recognized in the geology and generally interpreted as a left-lateral strike-slip fault (Scientists of the U.S. Geological Survey and the Southern California Earthquake Center, 1994; Seeber and Armbruster, 1995a). The 1994 aftershocks indicate that the Northridge thrust is continuous across the Chatsworth trend. There are secondary corrugations (Fig. 4b) east of the ramp that are parallel to it and have a wavelength of about 4 km. Corrugations of 'thread geometry' on fault surfaces seem to be a rather common feature and exist at different scales, as shown by Thibaut et al. (1996). A thread surface, of which the contact surface between a nut and bolt is an example, is defined as a surface tangent to a non-zero twistor vector field, and in nature it can be created when two rigid blocks slip past each other (Thibaut et al., 1996). The grooves and striae on a fault surface are therefore comparable with the field lines of the twistor field (Thibaut et al., 1996).

Our 3-D model of the Northridge thrust enables us to further examine the relationship between fault geometry and rupture propagation. For this, we have mapped the Northridge slip model of Wald et al. (1996) — which they computed on a dipping plane oriented approximately the same as our Northridge thrust surface — onto our 3-D corrugated fault model (Fig. 5). The 1994 main-shock hypocenter was located near the bottom of the lateral ramp (along the ridge of the main corrugation). The 1994 rupture did not propagate much east of the lateral ramp, but rather began on it, and propagated westward and upward (Fig. 5). This suggests that the presence of lateral ramps and corrugations can control the propagation of the fault rupture during an earthquake and ultimately limit the earthquake size.

Our model of the Northridge thrust also highlights the importance of corrugated fault geometry in controlling how the two fault blocks slip relative to each other, and the usefulness of 3-D fault surfaces for predicting slip directions. West of the lateral ramp, the slip directions computed by Mallet et al. (1999) on the basis of the principal curvatures of our fault geometry alone (Fig. 6a) are similar to the seismologically constrained slip model of Wald et al. (1996) (Fig. 5a). Furthermore, if we compare the aftershock focal mechanisms with the corrugations (Fig. 6b–d), we notice that the trend and plunge of the mean slip direction of the aftershocks also are nearly identical to the mean trend and plunge of the corrugations. This further supports our hypothesis that the orientation of the corrugations is controlling the range of possible slip motions on the Northridge thrust. These results complement those of Thibaut et al. (1996), who showed that it is possible to constrain fault geometry knowing the slip vector and assuming faults to be optimized threaded surfaces.

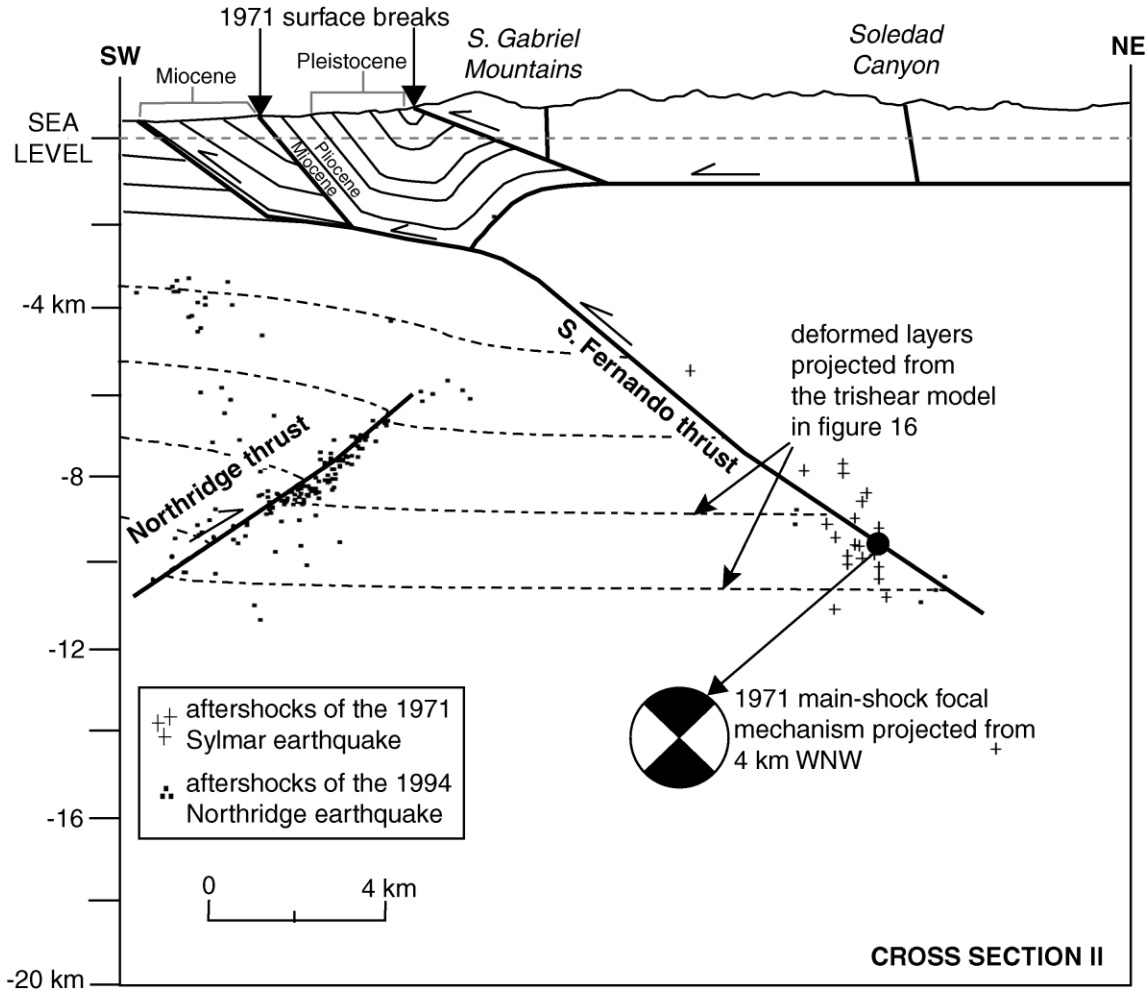

Fig. 12. Cross-section through the rupture of the 1971 Sylmar earthquake. The fold and fault geometries shown here are based on the fault models that we obtained from the earthquakes as well as from bed dips and fault traces extracted from geological maps (Dibblee, 1991). Location of cross-section is in Fig. 13.

4. Northridge thrust, San Fernando thrust, and surface folding

To obtain more information on possible interactions between the Northridge thrust and other nearby faults, we also modeled the San Fernando thrust from the aftershocks of the 1971 Sylmar earthquake. Data quality is not as good as for the 1994 Northridge earthquake, and fewer lower magnitude events were recorded because of the less dense and accurate seismic network in place at the time of the 1971 earthquake. However, there are clear surface breaks from the 1971 earthquake that can be used as additional constraints for the fault model.

The aftershock hypocenters do not satisfy all the requirements for the application of the clustering method (Appendix A). Therefore, we modeled the San Fernando thrust surface from the original, unclustered locations, in combination with aftershock focal mechanisms and surface breaks. The resulting model surface is less detailed than the one we obtained for the Northridge thrust (Fig. 7 shows a very small difference between the 3-D surface fit and the least-squares fit for the San Fernando thrust), but we were able to determine the strike, dip, and the maximum depth of the thrust, as well as any major changes in them. In our initial 3-D model, the San Fernando thrust is defined as a single surface with an approximately constant dip and strike below a depth of 8 km (Figs. 8 and 9). Whitcomb et al. (1973) suggested the presence of a lateral ramp on the San Fernando thrust to explain strike-slip mechanisms on the western side of the aftershock zone. Our model indicates that there are indeed changes in the strike of the fault, at least above a depth of 8 km, although a detailed geometry cannot be determined from the aftershock locations because of their scattering.

Several different models have been proposed for the geometry of this thrust and to explain the surface breaks. Whitcomb et al. (1973), Sharp (1975), Langston (1978), Heaton (1982), and Tsutsumi and Yeats (1999) present a series of different interpretations. As Tsutsumi and Yeats (1999) observe, “The variety of these models indicates that considerable uncertainty still exists regarding the fault geometry and slip history during the 1971 earthquake”. It is

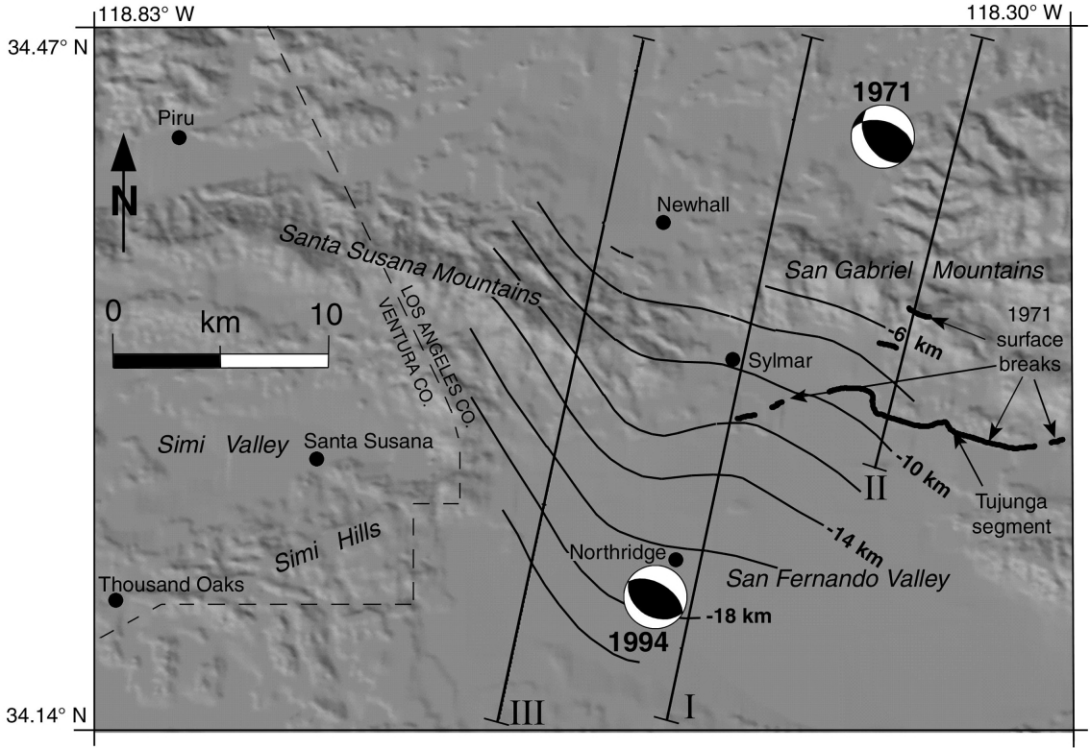

Fig. 13. Shaded-relief (USGS DEM) location map for the cross-sections in Figs. 10, 12 and 14. This figure also shows the depth contours (contour interval = 2 km) of the Northridge thrust, the surface breaks of the 1971 Sylmar earthquake, and the focal mechanisms of the 1971 Sylmar earthquake and of the 1994 Northridge earthquake. Note the hills on the northern side of the 1971 surface breaks (Tujunga segment).

not surprising that several fault geometries illustrated in these papers are incompatible with some of the presently available data, as we discuss below.

There are very few earthquakes at depths between 0 and 4 km, therefore we require a solution that takes into account both the hypocentral locations, and the near-surface geological data, including the surface breaks. The sources of geological data that we used were published papers (Yeats and Huftile, 1995; Huftile and Yeats, 1996), geological maps (Dibblee, 1991, 1992a,b, 1996), and a series of N–S and E–W seismic reflection profiles from the oil industry. The near-surface data tell us that a single planar fault, or any fault with constant dip in the top 3–4 km (Whitcomb et al., 1973; Heaton, 1982), is not a viable solution, because it cannot account for the steeply dipping layers at the western foot of the San Gabriel Mountains and the bedding-parallel thrusting on faults in this same area. Our solution (shown in Figs. 10–12) is similar to a solution presented by Tsutsumi and Yeats (1999), although we differ in the interpretation of the surface breaks. According to these authors, the surface breaks are most likely secondary features produced by flexural-slip folding; this solution is plausible in the location of their section, but not viable for our particular sections where the surface breaks lie along mapped surface faults. The solution we present in Fig. 12 shows that most of the surface breaks are produced by slip along a bedding-parallel thrust fault that connects at a depth of 2 km with the main San Fernando thrust. This would explain why most of the breaks (Tujunga segment; Tsutsumi and Yeats, 1999) occur at the foot of a hill (visible in the shaded-relief map of Fig. 13), whose topographic relief is most likely due to repeated slip along a fault located exactly where the breaks occurred.

It should also be noted that there are large N–S changes in Upper Tertiary stratigraphic thicknesses in this region (Dibblee, 1991, 1992a), which prevent detailed stratigraphic correlation across fault blocks. This fact suggests that the shallow faults, and possibly the deeper San Fernando thrust itself, are reactivating old normal faults of the southern margin of the Ventura basin (see also Yeats et al., 1994; Huftile and Yeats, 1996; Tsutsumi and Yeats, 1999).

As first noted by Mori et al. (1995), the San Fernando thrust cuts off (or overlies) the top of the Northridge thrust at its eastern end at a depth of 5–6 km (Figs. 8 and 9). The cut-off relationship between the Northridge thrust and the Santa Susana fault, however, is more ambiguous. When we superimpose a shaded-relief map over the fault depth-contours of the Northridge thrust (Fig. 13), it is apparent that both thrusts are overlain at least in part by a mountain range, specifically the Santa Susana Mountains for the Northridge thrust and the San Gabriel Mountains for the San Fernando thrust.

In Figs. 10, 12 and 14, we combined the aftershocks, the near-surface geological data (Fig. 15), and slices of our

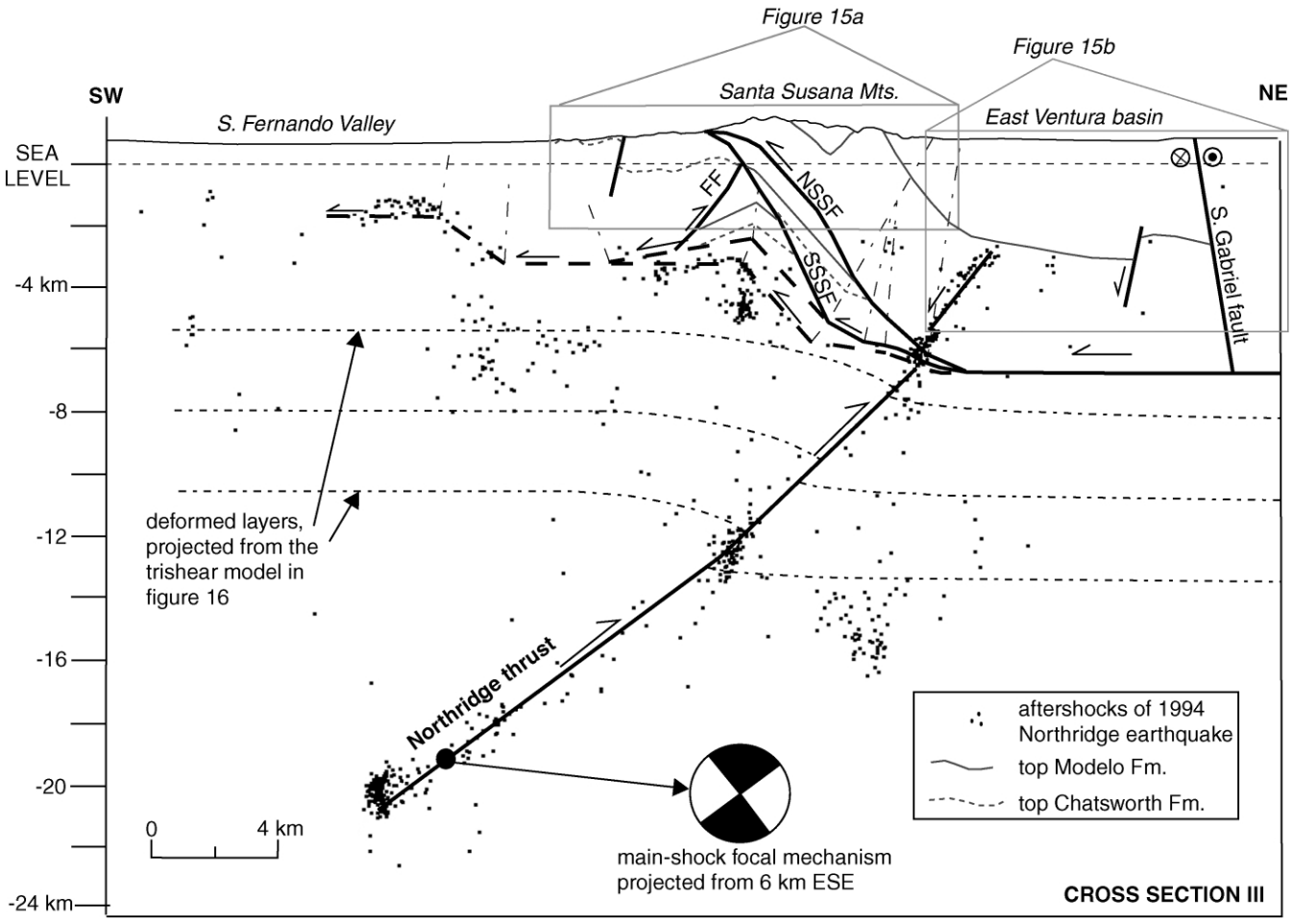

Fig. 14. Cross-section through the San Fernando Valley, Santa Susana Mountains, and East Ventura basin. The aftershocks of the 1994 Northridge earthquake are projected from a distance of 1 km on each side of the section. The near-surface structures are based on the geological maps of Dibblee (1992a) (Fig. 15a) and a cross-section from Huftile and Yeats (1996) (Fig. 15b). NSSF = Santa Susana fault, north strand; SSSF = Santa Susana fault, south strand; FF = Frew fault. Location of cross-section is in Fig. 13.

modeled surfaces for the Northridge thrust and the San Fernando thrust to produce cross-sectional interpretations of the area. Note that the earthquakes have been projected onto the sections, and this is why the geometry they outline does not necessarily coincide with the slices of the modeled thrust surfaces.

Fig. 14 shows yet another example of the importance of 3-D modeling. Earthquakes that fall near the updip projection of the Northridge thrust between 3 and 5 km depth (Fig. 14) have been previously interpreted as a steepening of the thrust itself in this region (Unruh et al., 1995). We instead interpret them as occurring on a separate Miocene normal fault, whose existence is reported by Huftile and Yeats (1996). In fact, when this cluster of earthquakes is viewed in 3-D, not only is its dip steeper than that of the Northridge thrust immediately below it, but the strike azimuth also differs by more than 10° (it is closer to 130° than to 110°). Considering the relative depths and orientations of the two clusters, it would not be possible to fit a continuous surface between them, as it would create a jog in the fault incompatible with thrust motion.

On the sections in Figs. 10, 12 and 14, we also superimposed formlines of a trishear fault-propagation fold model (Fig. 16; Erslev, 1991; Hardy and Ford, 1997; Allmendinger, 1998) of the deformation attributed to the Northridge thrust, as discussed below.

5. Modeling Northridge folding: the trishear model

We seek to evaluate how shallow folding might be caused by the Northridge thrust. Three possible folding mechanisms are shown schematically in Fig. 17 (fault-propagation folding, Suppe and Medwedeff, 1990; wedge structure, e.g. Medwedeff, 1992; and trishear fault-propagation folding, Erslev, 1991). The Northridge thrust lies largely in the basement and does not show any major dip changes in section. Classical fault-propagation folding (proposed for the Northridge thrust by Davis and Namson, 1994), or a shallow wedge structure, can both explain the steep north dips under the Santa Susana thrust in the westernmost section (Figs. 14 and 15), but they seem difficult to reconcile with

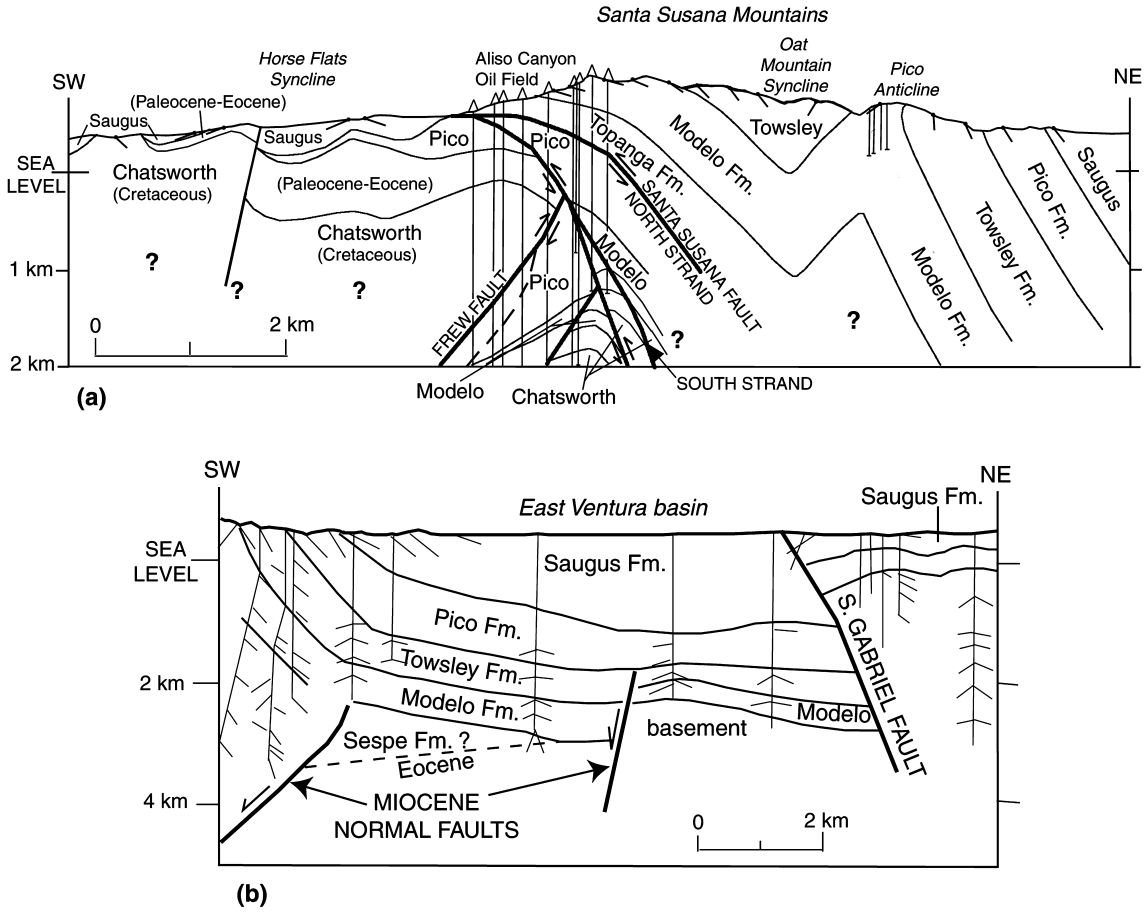

Fig. 15. (a) Cross-section through the Santa Susana Mountains, modified after Dibblee (1992a). (b) Cross-section through the East Ventura basin, modified after Huftile and Yeats (1996).

other geometrical characteristics of the Northridge thrust and the overlying structure, for reasons given below. In contrast, the trishear mechanism seems possible, but it requires a different explanation for the steep dips below the Santa Susana thrust.

A classical fault-propagation folding mechanism requires an associated synclinal fault bend, stepping up either from a

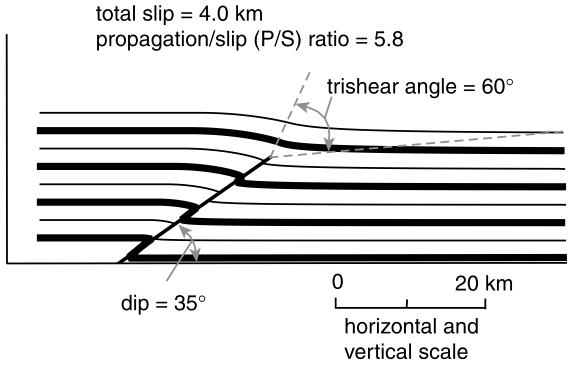

Fig. 16. 2-D trishear model for the Northridge thrust obtained with Trishear PPC 3.0 (Allmendinger, 1999). The azimuth of the section is 3° E, which is the long-term slip direction of the thrust (the choice of parameters for this model is explained in the text).

decollement as shown in Fig. 17a, or from a less steeply-dipping fault (Suppe and Medwedeff, 1990). There is no direct evidence for such a bend, which would produce steep regional back dips not directly observed in the available data. The solution of Davis and Namson (1994) contains this backlimb in a location where it would be hidden. A backlimb is not required for the wedge or trishear solutions, but is admissible. Classical fault-propagation folding also requires the branching of the anticlinal crest at the same layer as the fault tip (Fig. 17a), which seems difficult to accommodate with the fault tip determined from aftershocks and from the positions of the anticline and possible backlimb. Thus, we will not consider the classical fault-propagation fold mechanism further, even though we have applied it elsewhere on the south flank of the Ventura Basin (Suppe and Medwedeff, 1990).

Wedge solutions (such as shown schematically in Fig. 17b, with an independent south-vergent Santa Susana roof thrust) require the fault to flatten under the anticline to a detachment, with slip wedging back onto the preexisting south-vergent roof thrust. In the western section (Fig. 14), the Northridge thrust projects up into the syncline north of the Santa Susana Mountains rather than into the anticline under the Santa Susana thrust. Therefore wedge solutions

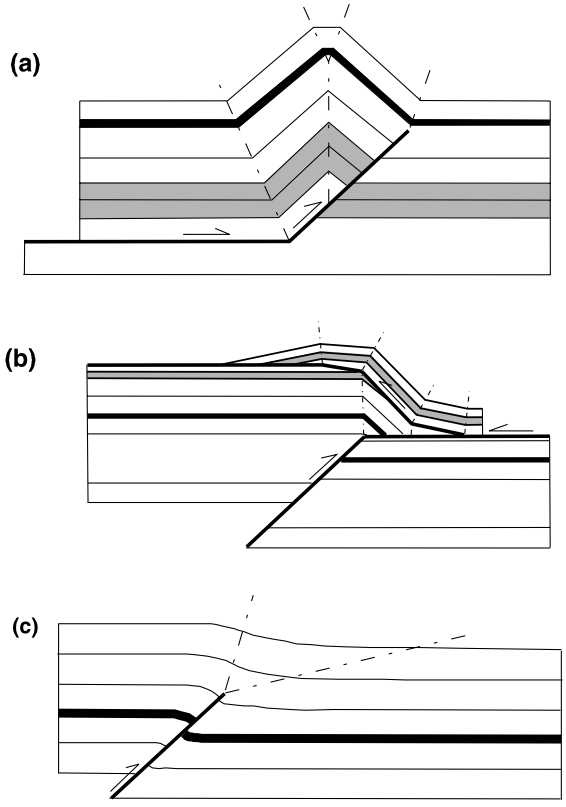

Fig. 17. Models considered to explain the fault and fold geometries beneath the Santa Susana Mountains with respect to the position of the Northridge thrust. (a) Classical fault-propagation folding; the thrust ramp terminates at the syncline and an extensive backlimb must be present. (b) Wedge structure; the thrust ramp terminates at the anticline and a backlimb need not exist. (c) Trishear fault-propagation folding; the thrust tip terminates at the syncline and a backlimb need not exist.

are not an attractive mechanism for generating the anticline or the south-vergent structures. Previous works have interpreted the shallow south-vergent structure as independent of the Northridge fault (Davis and Namson, 1994; Yeats and Huftile, 1995; Huftile and Yeats, 1996), which we follow here (Figs. 10–14).

Inasmuch as the Northridge thrust is blind, slip must go to zero at its tip, which requires associated folding. Furthermore, there is no appreciable change in fault dip. Therefore, a trishear fault-propagation fold mechanism (Fig. 17c) seems attractive (Erslev, 1991; Hardy and Ford, 1997; Allmendinger, 1998). The trishear mechanism also has been successfully applied to the nearby well-imaged structure of the Puente Hills–Whittier Narrows basement-involved blind thrust system of the northern Los Angeles basin (Shaw and Shearer, 1999; Allmendinger and Shaw, 2000). Trishear fault-propagation folding does not require the presence of any decollement, regional back dips, or shallowing of the thrust dip near its upper termination, and the updip projection of the thrust terminates at the syncline. It also produces much less evident deformation, with gentle dips localized in a narrow area updip from the thrust, which could explain why it is so difficult to find any clear folding at the surface that can be unequivocally associated with the Northridge thrust. The steep dips below the Santa Susana Mountains in the western section (Fig. 14) would require some independent explanation, for example, by footwall imbrication of the Santa Susana system as shown schematically in our section or by back thrusting of the Frew fault (Dibblee, 1992a; Huftile and Yeats 1996), or both. This deformation style is consistent with that elsewhere in the San Fernando Valley (Figs. 10–12); for example, the Northridge Hills anticline produced by one of these shallow, southward-imbricating thrusts, which is imaged in seismic-reflection profiles (Fig. 11; see also Tsutsumi and Yeats, 1999). Steeply-dipping beds that can be linked to imbricating thrusts exist at the foot of the San Gabriel Mountains (Figs. 10 and 12). This south-vergent solution would also explain the presence of sub-horizontal clusters of seismicity at shallow depths (Fig. 14).

Fig. 16 illustrates the trishear model for the Northridge thrust that we produced using the TrishearPPC software (Allmendinger, 1999). In order to simplify the calculations, we assumed that the slip happened along a direction of azimuth 3° E in a single episode, and that the total slip is constant along strike. In our trishear model we used the total slip of 4.0 km calculated by Huftile and Yeats (1996).

The use of a 3° E slip direction is supported by the fact that this is also the trend of the corrugations on the thrust surface, as explained in Section 3.2, and thus the most likely long-term slip direction (Fig. 6b–d). We did not use the slip direction of the main-shock focal mechanism because it represents slip for initial rupture only (Fig. 5a), and it cannot be considered representative of the long-term slip.

Applying the slip all at once means that we are not taking into account possible interactions with other faults slipping at the same time, which can give rise to more complex geometries than those we were able to model. We have no information on how slip episodes on different faults in the area are distributed in time and space, and thus we cannot model these more complex details.

A constant slip of our model implies that the strike of the axial planes of the folds generated by slip on the thrust are parallel to the strike of the thrust itself. This is a simplification, because it is likely that slip varies along strike, especially near the lateral edges of the fault and between the two regions E and W of the lateral ramp. In particular, Yeats and Huftile (1995) pointed out that slip decreases by more than half from W to E going from the Oak Ridge fault to the Northridge thrust, and Tsutsumi and Yeats (1999) notice that structural relief decreases in the eastern San Fernando Valley. Keeping this observation in mind, and noting that the projected slip from Wald et al. (1996) (Fig. 5b) is located mostly W of lateral ramp, we think that the total slip could be decreasing from W to E of the lateral ramp on the Northridge thrust. However, we have no means of knowing how much smaller the total slip is to the E of the lateral ramp, thus we produce a constant-slip,

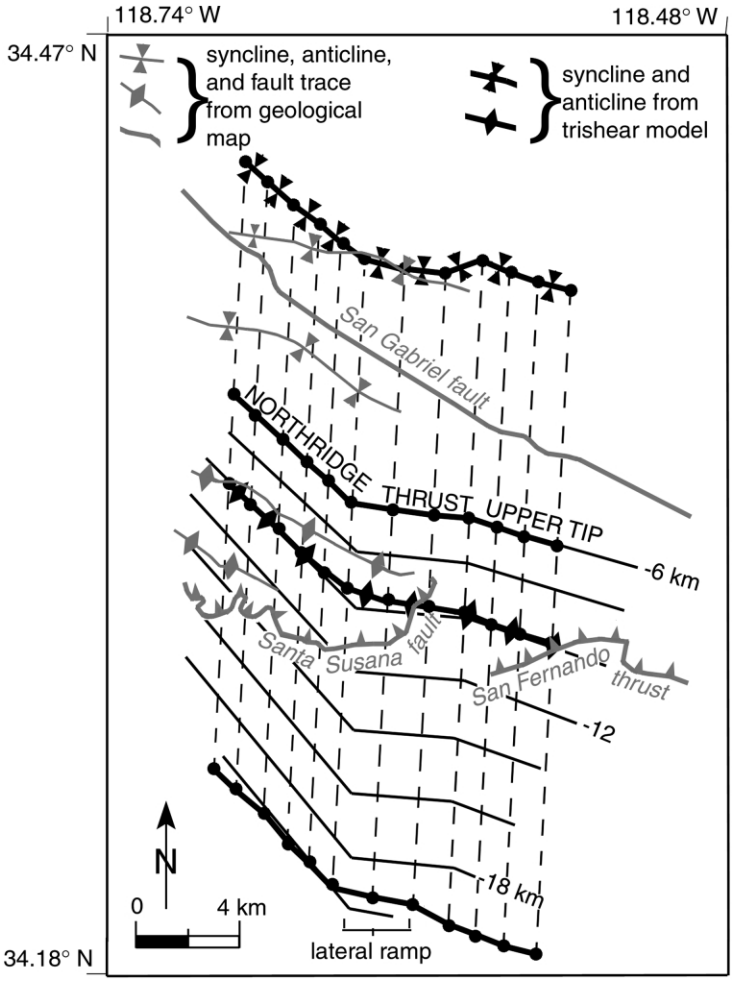

Fig. 18. Map that compares the position of several field structures with those in the constant-slip end-member, pseudo-3D model obtained by aligning 12 identical, 2-D, trishear fault-propagation fold models (Fig. 16) of the Northridge thrust (dashed lines). We positioned the 2-D trishear sections by using the Northridge thrust upper and lower tips as guidelines, placing the sections parallel to the long-term slip direction of the thrust (see text for details).

end-member model that will then be useful for comparing qualitatively with the actual geology.

The fault dip that we use for the trishear model is 35°, which is the apparent dip in the slip direction at any point along the strike of the Northridge thrust. With the upper tip of the Northridge thrust as the reference line, we created 12 trishear cross-sections (Figs. 16 and 18) in order to obtain a pseudo-3D reconstruction of the geometry produced by slip along this fault (Fig. 19).

West of the lateral ramp, the anticline produced by our trishear model coincides with the anticlinorium of the Santa Susana Mountains recognizable from the geological data (Figs. 14 and 18). When compared with the trishear model, the field syncline between the Santa Susana Mountains and the San Gabriel fault is located at the updip projection of the modeled Northridge thrust. Imbricate thrusts to the SW are a plausible explanation for the abnormally high dip of the Santa Susana fault (Fig. 14), particularly because the ramp of the Santa Susana fault is probably a reactivated normal fault, as pointed out by Huftile and Yeats (1996).

East of the lateral ramp there is no obvious field anticline in the eastern San Fernando Valley (although there is evidence of folding of the overlying south-vergent thrusts; Figs. 10–12; Tsutsumi and Yeats, 1999), which is consistent with lower slip to the East. In this area, the main south-vergent thrust is the San Fernando thrust, which is deforming a higher thrust system, and is likely connected to the imbricate thrusts to the SW below the San Fernando Valley at shallow depth.

6. Conclusions

The combination of earthquake data and geological data allowed us to model in detail the geometry of the blind Northridge thrust and to conclude that it only contributes gentle surface folding due to trishear fault propagation. It seems unlikely that this folding alone could have allowed the identification of the Northridge thrust before 1994, because the complex deformation of the area masks it to a large degree and a 3-D fault model was not available at the

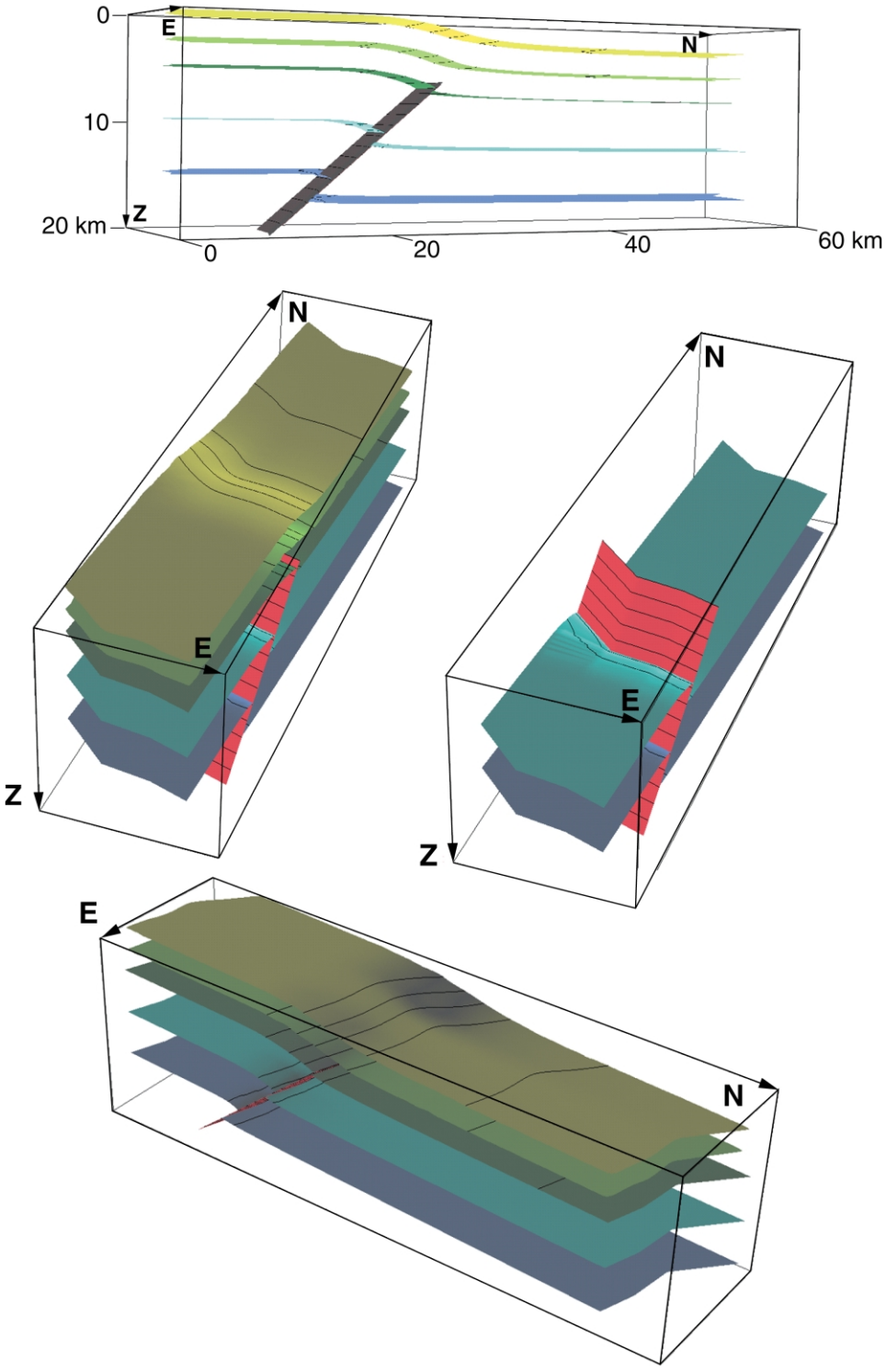

Fig. 19. Perspective views of the pseudo-3D trishear model. The layers are intended to illustrate the deformation only, not to represent any specific stratigraphic horizons. The fault is in red.

time. Under these conditions, connecting a particular fold to a blind thrust is difficult. Without using earthquake data, the only realistic way that the presence of the Northridge thrust could have been detected before 1994 was, as explained by Yeats and Huftile (1995), by noticing the uplift in the footwall of the Santa Susana fault.

However, we believe that (1) a reasonable 3-D image of the fault could have been obtained before 1994 from

background seismicity event locations and focal mechanisms (Seeber and Armbruster, 1995a; Carena and Suppe, 1999a), and (2) the method that we developed can help identify dangerous faults in other cases, as 3-D models can be created from existing earthquake catalogs and compared with near-surface and surface structures. Furthermore, existing seismic networks could be optimized to record seismicity to much lower magnitudes, thereby providing orders of magnitude more earthquakes for the imaging of active structures.

The most striking feature of the imaged fault is mega-corrugations oriented parallel to the mean aftershock slip direction, with most of the 1994 slip confined to the west of the largest corrugation (the lateral ramp). This observation supports the concept that faults are 3-D threaded surfaces whose relative displacement is close to parallel to the grooves, as proposed by Thibaut et al. (1996).

Acknowledgements

Thanks to R. Jones for running his collapsing code on our aftershock sets, and to R. Allmendinger for providing his TrishearPPC 3.0 code. The data that we used are from the Southern California Seismic Network for the phase and catalog data and SCEC_DC for the focal mechanisms (with data provided by N. Seeber). Thanks to E. Hauksson for providing the velocity model that we used to recompute the locations of the Northridge aftershocks from the phase data. We also would like to thank M.S. Wilkerson, A. Meigs, and J. Namson for their helpful reviews. This research was supported in part by the National Earthquake Hazards Reduction Program of the US Geological Survey, Grant Number 01HQGR0028.

Appendix A

Hypoinverse (Klein, 1978, 1989) is software routinely used in seismology to locate earthquakes. Both program and user manual are freely available for research purposes from the Southern California Earthquake Center (SCEC).

To calculate the earthquake locations, we used the following information as input data for Hypoinverse, the 2-D velocity model given below, which was derived from the 3-D model of Hauksson (1997):

Velocity (km/s)	Depth (km)
4.80	0.00
5.78	4.00
6.15	6.00
6.30	8.00
6.44	12.00
6.54	16.00
6.72	20.00
7.76	32.00

In this way, we obtained the location error ellipsoids of the earthquake hypocenters, which are otherwise not recorded in the SCEC earthquake catalog. We needed this information in order to relocate the earthquakes with the Jones and Stewart (1997) 'collapsing' or *clustering method*. This method is based on the assumption of simplicity: one fault slipping twice is a simpler explanation for the occurrence of two overlapping events than two separate faults each slipping once. The algorithm searches for earthquakes that fall within the error ellipsoid of another earthquake, and moves those events closer together, so that events 'collapse' in tight clusters. It can be applied whenever (1) the events were recorded by a local network; (2) information about location errors exists; and (3) the earthquake clouds are dense enough that there is significant overlap between earthquake error ellipsoids. See Jones and Stewart (1997) for details of the method and discussion of errors.

We selected the clustering method instead of other possibly more accurate relocation methods like waveform comparison (e.g. Got et al., 1994; Rubin et al., 1999a,b) because, for the level of detail we were seeking, clustering was still the best compromise between accuracy and speed. Moreover, such methods have stricter criteria for choosing events suitable for relocation, with the inevitable result that a substantial number of events are discarded, with significant loss of information. In fitting optimized planes to points, however, the accuracy in location of an event is not as important as having large numbers of events.

References

Allmendinger, R.W., 1998. Inverse and forward numerical modeling of trishear fault-propagation folds. Tectonics 17 (4), 640–656.

Allmendinger, R.W., 1999. TrishearPPC, 3.0. Ithaca, New York.

Allmendinger, R.W., Shaw, J.H., 2000. Estimation of fault propagation distance from fold shape: Implications for earthquake hazard assessment. Geology 28 (12), 1099–1102.

Brankmann, C.M., 1995. Relative relocation of aftershocks of the 1994 Northridge California Earthquake. BS thesis, Princeton University.

Carena, S., 1999. 3-D imaging of faults using aftershocks of large earthquakes. EUG 10 Journal Conference Abstracts 4, 455.

Carena, S., Suppe, J., 1999a. The importance of small earthquakes and good locations in the hunt for blind faults: the example of Northridge. Eos, Transactions, American Geophysical Union 80 (46, Suppl.), 644.

Carena, S., Suppe, J., 1999b. 3-D structure of the Northridge area. Abstracts with Programs, Geological Society of America 31, 7.

Carena, S., Suppe, J., Kao, H., 2000. How the 1999 Chi–Chi, Taiwan earthquake helped reveal the structure beneath Central Taiwan. Eos, Transactions, American Geophysical Union 81 (48, Suppl.), 883.

Davis, T.L., Namson, J.S., 1994. A balanced cross-section of the 1994 Northridge earthquake, southern California. Nature 372, 167–169.

Dibblee, T.W., Jr, 1991. Geologic map of San Fernando and Van Nuys (north 1/2) quadrangles, Los Angeles County, California, Dibblee Geological Foundation Map DF-33, scale 1:24,000.

Dibblee, T.W., Jr, 1992. Geologic map of the Oat Mountain and Canoga Park (north 1/2) quadrangles, Los Angeles County, California, Dibblee Geological Foundation Map DF-36, scale 1:24,000.

Dibblee, T.W., Jr, 1992. Geologic map of the Santa Susana quadrangle, Ventura and Los Angeles Counties, California, Dibblee Geological Foundation Map DF-38, scale 1:24,000.

Dibblee, T.W., Jr, 1996. Geologic map of the Newhall quadrangle, Los Angeles County, California, Dibblee Geological Foundation Map DF-56, scale 1:24,000.

Erslev, E.A., 1991. Trishear fault-propagation folding. Geology 19 (6), 617–620.

Gocad Consortium, 2000. http://www.ensg.u-nancy.fr/GOCAD/consortium.html

Got, J.L., Frechert, J., Klein, F.W., 1994. Deep fault plane geometry inferred from multiplet relative relocation beneath the south flank of Kilauea. Journal of Geophysical Research 99, 15375–15386.

Hardy, S., Ford, M., 1997. Numerical modelling of trishear fault-propagation folding and associated growth strata. Tectonics 16 (5), 841–854.

Hauksson, E., 1997. Three-dimensional Vp and Vp/Vs velocity models of Southern California. Seismological Research Letters 68 (2), 321.

Heaton, T.H., 1982. The 1971 San Fernando earthquake: a double event? Bulletin of the Seismological Society of America 72, 2037–2062.

Huftile, G.J., Yeats, R.S., 1996. Deformation rates across the Placerita (Northridge Mw = 6.7 aftershock zone) and Hopper Canyon segments of the Western Transverse Ranges deformation belt. Bulletin of the Seismological Society of America 86, S3–S18.

Jones, R.H., Stewart, R.C., 1997. A method for determining significant structures in a cloud of earthquakes. Journal of Geophysical Research 102, 8245–8254.

Klein, F.W., 1978. Hypocenter location program HYPOINVERSE Part 1, Users guide to versions 1, 2, 3 and 4; Part 2, Source listings and notes. U.S. Geological Survey Open-File Report 78-694, 114pp.

Klein F.W, 1989. User's guide to HYPOINVERSE, a program for VAX computers to solve for earthquake locations and magnitudes. U.S. Geological Survey Open-File Report 85-0515, 58pp.

Langston, C.A., 1978. The February 9, 1971 San Fernando earthquake: a study of source finiteness in teleseismic body waves. Bulletin of the Seismological Society of America 68, 1–29.

Mallet, J.L., 1992. Discrete smooth interpolation in geometric modelling. Computer Aided Design 24, 178–191.

Mallet, J.L., 1997. Discrete modeling for natural objects. Mathematical Geology 29 (2), 199–219.

Mallet, J.L., Massot, J., Cognot, R., 1999. Fault characterization. Proceedings of the 19th Gocad Meeting, Nancy School of Geology, Nancy, France, June 14–17, 1999. ASGA (Association Scientifique pour la Géologie et ses Applications).

Medwedeff, D., 1992. Geometry and kinematics of an active, laterally propagating wedge thrust, Wheeler Ridge, California. In: Mitra, S., Fisher, G.W. (Eds.). Structural Geology of Fold and Thrust Belts. Johns Hopkins Univ. Press, Baltimore, pp. 3–28.

Mori, J., Wald, D.J., Wesson, R.L., 1995. Overlapping fault planes of the 1971 San Fernando and 1994 Northridge, California earthquakes. Geophysical Research Letters 22, 1033–1036.

Rubin, A.M., Gillard, D., Got, J.L., 1999a. Fault fabrics/earthquake mechanics from precise relative earthquake locations. Seismological Research Letters 70, 246.

Rubin, A.M., Gillard, D., Got, J.L., 1999b. Streaks of microearthquakes along creeping faults. Nature 400, 635–641.

Scholz, C.H., 1990. The Mechanics of Earthquakes and Faulting. Cambridge University Press, Cambridge.

Scientists of the U.S. Geological Survey and the Southern California Earthquake Center, 1994. The magnitude 6.7 Northridge, California, earthquake of 17 January 1994. Science 266, 389–396.

Seeber, N., Armbruster, J., 1995a. Faults and stress from earthquakes in southern California. Southern California Earthquake Center 1994 Annual Report, (Southern California Earthquake Center, Los Angeles, CA), vol. II, F37–F38.

Seeber, N., Armbruster, J., 1995b. The San Andreas fault system through the Transverse Ranges as illuminated by earthquakes. Journal of Geophysical Research 100, 8285–8310.

Sharp, R.V., 1975. Displacement on tectonic ruptures. In: Oakeshott, G.B. (Ed.). San Fernando, California Earthquake of 9 February 1971. California Division of Mines and Geology Bulletin, pp. 187–194.

Shaw, J.H., Shearer, P.M., 1999. An elusive blind-thrust fault beneath metropolitan Los Angeles. Science 283, 1516–1518.

Shaw, J.H., Bischke, R.E., Suppe, J., 1994. Relations between folding and faulting in the Loma Prieta epicentral zone: strike-slip fault-bend folding. In: Simpson, R.W. (Ed.), The Loma Prieta, California, Earthquake of October 17, 1989: Tectonic Processes and Models. U.S. Geological Service Professional Paper 1550, F3–F21.

Southern California Earthquake Center, 1994. http://www.scec.org.

Suppe, J., 1983. Geometry and kinematics of fault-bend folding. American Journal of Science 283, 684–721.

Suppe, J., Medwedeff, D., 1990. Geometry and kinematics of fault-propagation folding. Eclogae Geologicae Helvetiae 83, 409–454.

Thibaut, M., Gratier, J.P., Leger, M., Morvan, J.M., 1996. An inverse method for determining three-dimensional fault geometry with thread criterion: application to strike-slip and thrust faults (Western Alps and California). Journal of Structural Geology 18, 1127–1138.

Tsutsumi, H., Yeats, R.S., 1999. Tectonic setting of the 1971 Sylmar and 1994 Northridge earthquakes in the San Fernando Valley, California. Bulletin of the Seismological Society of America 89, 1232–1249.

Unruh, J.R., Twiss, R.J., Hauksson, E., 1997. Kinematics of postseismic relaxation from aftershock focal mechanisms of the 1994 Northridge, California earthquake. Journal of Geophysical Research 102, 24589–24603.

Van Dusen, A.B., 1997. Determining three-dimensional fault shape from earthquake hypocenters; an assessment of *Gocad* in modelling a fault surface with application to the June 28, 1992, Landers, California, earthquake. BA thesis, Princeton University.

Wald, D.J., Heaton, T.S., Hudnut, K.W., 1996. The slip history of the 1994 Northridge, California, earthquake determined from strong ground motion, teleseismic, GPS, and leveling data. Bulletin of the Seismological Society of America 86, S49–S70.

Whitcomb, J.H., Allen, C.R., Garmany, J.D., Hileman, J.A., 1973. San Fernando earthquake series 1971: focal mechanisms and tectonics. Reviews of Geophysics and Space Physics 11, 693–730.

Yeats, R.S., Huftile, G.J., Stitt, L.T., 1994. Late Cenozoic tectonics of the east Ventura basin, Transverse Ranges, California. AAPG Bulletin 78 (7), 1040–1074.

Yeats, R.S., Huftile, G.J., 1995. The Oak Ridge fault system and the 1994 Northridge earthquake. Nature 373, 418–420.